

1 Technical Communication

2 Magnesium Green for fluorometric measurement 3 of ATP production does not interfere with 4 mitochondrial respiration

5 Luiza HD Cardoso*, Carolina Doerrier, Erich Gnaiger

6 Oroboros Instruments, Innsbruck, Austria

7
8 *Corresponding author: luiza.cardoso@orooboros.at

9 Abstract

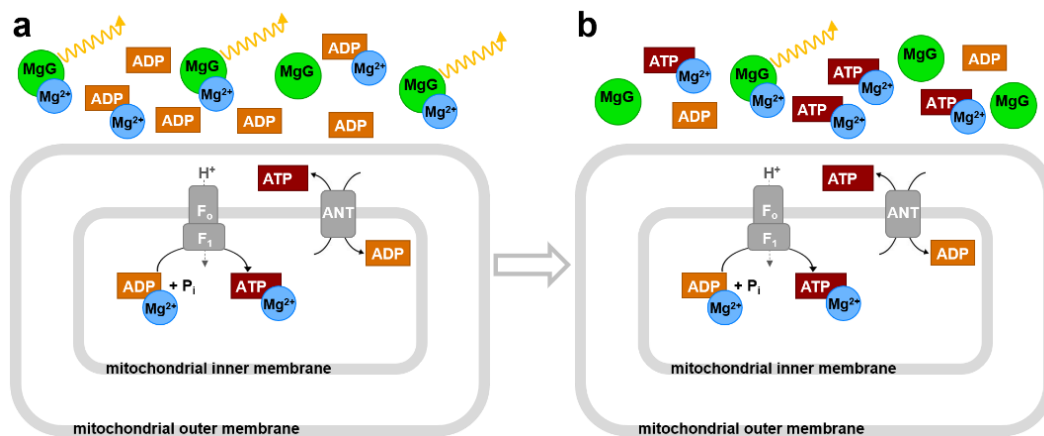
10
11 **For the advanced study of mitochondrial function, high-resolution respirometry is**
12 **extended by fluorometric measurement of ATP production using the fluorophore**
13 **Magnesium Green™ (MgG). A common problem with several fluorescent dyes is the**
14 **inhibition of mitochondrial respiration. In the present study, a coupling control protocol**
15 **was applied in combination with MgG to measure ATP production simultaneously with**
16 **respiration for calculation of P_o/O₂ ratios. MgG at 1.1 μM did not affect respiration through**
17 **the NADH-linked and succinate-linked pathways. Respiration was not inhibited in any of**
18 **the coupling control states, hence coupling control efficiencies were not affected by MgG.**

19
20 *Keywords* – ATP; ATP production; high-resolution respirometry; Magnesium Green;
21 mitochondria; oxidative phosphorylation; fluorometry; FluoRespirometry

22 23 1. Introduction

24 Mitochondrial ATP production can be analyzed with a fluorometric technique using
25 Magnesium Green™ (MgG) as a fluorescent probe, as described by Chinopoulos et al
26 (2009). Application of the Mg²⁺-sensitive fluorophore as an indicator of ATP production
27 relies on the fact that ADP and ATP have different affinities for Mg²⁺ (Gnaiger, Wyss 1994;
28 Leyssens et al 1996; Budinger et al 1998). ADP is phosphorylated to ATP in the
29 mitochondrial matrix. In the phosphorylation system ADP/ATP and inorganic phosphate
30 P_i are exchanged stoichiometrically by the adenine nucleotide translocase ANT and the
31 phosphate carrier PiC. Under experimental conditions when ADP decreases while ATP
32 increases in the extramitochondrial milieu, the Mg²⁺ concentration declines due to the
33 higher affinity for Mg²⁺ of ATP than ADP (Figure 1). Therefore, the fluorometric assay with
34 the membrane-impermeant MgG provides a quantitative approach to analyze
35 mitochondrial ATP production. This method was developed further to measure
36 concomitantly mitochondrial ATP production and O₂ consumption in the Oroboros O2k-
37 FluoRespirometer which is an experimental system complete for high-resolution
38 respirometry including fluorometry (Chinopoulos et al 2014).

40 Fluorescent dyes are widely used to assess various parameters relevant in
 41 mitochondrial physiology. Safranin, rhodamine and its derivatives, such as TMRM, are
 42 frequently employed as reporters of the mitochondrial membrane potential $\Delta\Psi_p+$.
 43 However, all $\Delta\Psi_p+$ dyes have been shown to affect mitochondrial respiration (Scaduto,
 44 Grotjohann 1999). Like TPP⁺, safranin mainly affects the NADH (N)-linked pathway, the
 45 phosphorylation system, and to a smaller extent the succinate (S)-linked pathway
 46 (Krumshabel et al 2014). The effect of $\Delta\Psi_p+$ fluorescent probes can be explained since
 47 they accumulate in the mitochondrial matrix and thus possibly affect mitochondrial
 48 function.



50 **Figure 1. Concept of the MgG assay according to Chinopoulos et al (2014).** MgG
 51 fluoresces when bound to Mg²⁺. ADP and ATP compete for Mg²⁺ binding with different
 52 affinities; ATP has a higher affinity for Mg²⁺ compared to ADP. **(a)** Initial experimental
 53 conditions, when ADP is added, binding some Mg²⁺, and high MgG fluorescence drops slightly.
 54 **(b)** As the experiment proceeds, ADP is phosphorylated to ATP, which is
 55 exchanged for ADP by the adenine nucleotide translocase ANT. With increase in ATP in
 56 the extramitochondrial medium, more Mg²⁺ is bound to ATP, and MgG fluorescence
 57 decreases.

58
 59 It is important to note that another dye frequently used in mitochondrial physiology
 60 studies, Amplex UltraRed, employed to analyze H₂O₂ production, was shown to affect
 61 mitochondrial respiration even though the mitochondrial membranes are not permeable
 62 to this fluorophore (Makrecka-Kuka et al 2015). Therefore, it is important to analyze
 63 whether MgG affects mitochondrial respiration, despite the fact that mitochondrial
 64 membranes are not permeable to this fluorophore.

65
 66 In the present technical communication, we report the effect of MgG on
 67 mitochondrial respiration, which is the gold standard to evaluate mitochondrial function.
 68 This provides an important contribution towards further development of this method to
 69 analyze P_»/O₂ ratios in different mitochondrial preparations. The use of a coupling
 70 control protocol assessing O₂ consumption and MgG fluorescence allows for the
 71 evaluation of mitochondrial respiration and ATP production using NADH- and succinate-
 72 linked substrates in LEAK, OXPHOS- and ET-state, making it possible to obtain flux control
 73 efficiencies.

74 2. Materials and methods

75 2.1. Reagents

76 Magnesium Green was purchased from Invitrogen/Thermo Fisher Scientific (cat. N°
77 M3733). Antimycin A (cat. N° A8674), ATP (cat. N° A2383), CCCP (cat. N° C2759), malate
78 (cat. N° M1000), MgCl₂ 1 M (cat. N° M1028), oligomycin (cat. N° O4876), pyruvate (cat.
79 N° P2256), rotenone (cat. N° R8875), SF 6847 (cat. N° T182), and succinate (cat. N°
80 S2378) were obtained from Sigma Aldrich. ADP was acquired from Millipore (cat. N°
81 117105), and carboxyatractyloside from Calbiochem (cat. N° 216201).

82 ADP and ATP were diluted in deionized H₂O without addition of Mg²⁺ salts, pH was
83 adjusted to 6.9 with KOH. Magnesium Green, malate, succinate, carboxyatractyloside and
84 MgCl₂ were diluted in deionized H₂O whereas antimycin A, CCCP, oligomycin, rotenone
85 and SF 6847 were diluted in ethanol p.a. All solutions were aliquoted and stored at -20 °C,
86 except pyruvate, which was diluted in deionized H₂O fresh on the day of each experiment.
87

88 2.2. Animals

89 Wild-type C57BL/6N adult mice (*N*=3 per experimental group) were housed in the
90 animal facility of the Medical University of Innsbruck (maximum 5 mice per cage) and,
91 maintained at 22 °C with a controlled 12 h light/dark cycle. Mice were fed *ad libitum* with
92 free access to water. All procedures were conducted according to the Austrian Animal
93 Experimentation Act in compliance with the European convention for the protection of
94 vertebrate animals used for experimental and other scientific purposes
95 (Tierversuchsgesetz 2012; Directive 2010/63/EU; BMWFM-66.011/0128-
96 WF/V/3b/2016).

97 2.3. Cardiac mitochondrial isolation and protein concentration determination

98 Following cervical dislocation, the hearts were immediately excised and transferred
99 into ice-cold biopsy preservation solution (BIOPS: 10 mM Ca²⁺-EGTA - 0.1 μM free Ca²⁺,
100 20 mM imidazole, 20 mM taurine, 50 mM K⁺-MES, 0.5 mM dithiothreitol, 6.56 mM MgCl₂,
101 5.77 mM ATP, 15 mM phosphocreatine, pH 7.1 adjusted with KOH) for short period of
102 time (1–2 h; Fontana-Ayoub et al 2016). All procedures were performed on ice (Gnaiger
103 et al 2000a). Mouse heart mitochondria were isolated following the protocol described
104 by Fontana-Ayoub and Krumschnabel (2015). The heart (~ 80–120 mg) was washed to
105 remove blood clots and minced with 1 mL of BIOPS. The tissue was homogenized with 2
106 mL isolation buffer (IB1: 0.5 M mannitol; 0.5 M sucrose; 0.1 M EGTA; pH 7.4 adjusted with
107 Tris; 2.5 mg/mL BSA and 0.5 mg/mL subtilisin, the latter two added freshly on the day of
108 use) on a 10 mL glass-Teflon Potter Elvehjem homogenizer, 6–8 × with about 1000 rpm
109 mechanical rotation. 3 mL of IB1 was added to the homogenate which was centrifuged at
110 800 *g* for 10 min at 4 °C. The supernatant was centrifuged again, at 10 000 *g* for 10 min
111 at 4 °C. The pellet was resuspended carefully using a 1 mL pipette in 0.5 mL IB2 (IB1 without
112 subtilisin). After addition of 2 mL IB2, the homogenate was centrifuged again at 10 000 *g*
113 for 10 min at 4 °C. The pellet was resuspended in 200 μL of IB3 (IB1 without BSA and
114 subtilisin) and kept on ice until use on the same day within 2 h.
115
116
117
118
119
120

121 Protein concentration was used for calculation of mass specific O₂ flux, determined
 122 using the kit DC Protein Assay (Bio-Rad, Hercules, CA, US). Absorbance was measured at
 123 620 nm with a Tecan Infinite TM F200 spectrophotometer (Tecan, Männedorf,
 124 Switzerland), using BSA at different concentrations as standards (Lowry et al 1951).
 125

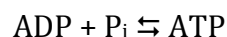
126 *2.4. High-resolution respirometry*

127
 128 Oxygen consumption and ATP production measurements were performed
 129 simultaneously at 37 °C in the O2k-FluoRespirometer (O2k, Oroboros Instruments,
 130 Innsbruck, Austria). The O2k includes two Duran® glass chambers with stirring (750
 131 rpm) and controlled temperature for closed-chamber respirometry using polarographic
 132 oxygen sensors (POS). Smart Fluo-Sensors Blue were used, with excitation LED 465 nm
 133 and filters for the LED and photodiode selected for Magnesium Green™). Specific
 134 amperometric emission and detection settings – fluorescence light intensity of 500 and
 135 gain 100 – were applied with the software DatLab 7.4 (Oroboros Instruments, Innsbruck,
 136 Austria) with continuous data recording set at 2 s time intervals. Standardized
 137 calibrations and instrumental O₂ background tests were performed (Doerrier et al 2018).
 138 The time-derivative of the O₂ concentration is calculated real-time by DatLab, providing
 139 traces of O₂ flux corrected for the O₂ instrumental background (Gnaiger 2001).
 140

141 Experiments were run with cardiac isolated mitochondria at protein concentrations
 142 in the range of 0.026–0.049 mg/mL in modified mitochondrial respiration medium
 143 MiR05-MgG (MgCl₂ 1 mM instead of 3 mM in MiR05, EGTA 0,5 mM, KH₂PO₄ 10 mM, Hepes
 144 20 mM, lactobionic acid 60 mM, D-sucrose 110 mM, taurine 20 mM, BSA 1 g/L, pH
 145 adjusted with KOH to 7.1). This modification of MiR05 (Gnaiger et al 2000a) was
 146 optimized for measurement of ATP production with MgG.
 147

148 *2.5. ATP production measurement with MgG*

149
 150 MgG (Magnesium Green™, pentapotassium salt, cell impermeant) does not
 151 permeate biological membranes. Therefore, the plasma membrane barrier function must
 152 be removed, as achieved in mitochondrial preparations – isolated mitochondria, tissue
 153 homogenates, permeabilized tissues and cells. MgG remains outside of the mitochondrial
 154 matrix and fluoresces when bound to Mg²⁺. In the phosphorylation reaction



156 reactants and MgG bind Mg²⁺ according to their apparent dissociation constants. When
 157 ADP is added to the experimental chamber, there is a fast drop of the fluorescence signal.
 158 If mitochondria and fuel substrates are present, ATP is generated and exchanged with
 159 ADP by the ANT. ATP has a higher affinity to Mg²⁺ compared to ADP. As ATP concentration
 160 increases in the medium, the free Mg²⁺ concentration declines, less MgG is bound to Mg²⁺,
 161 and the fluorescence decreases. The ATP concentration in the medium is calculated
 162 according to Chinopoulos et al (2009; 2014), taking in account that: (1) the initial
 163 concentration of ATP is zero, (2) the initial concentration of ADP is known, (3) the
 164 concentration of Mg²⁺ is measured, and (4) apparent *K_d* values for ADP and ATP with Mg²⁺
 165 are obtained experimentally.
 166

167 The free Mg^{2+} concentration was calibrated in MiR05-MgG containing the
168 mitochondrial sample, fuel substrates, carboxyatractyloside, and oligomycin. $MgCl_2$ was
169 titrated in 10 steps of 0.1 mM to obtain a non-linear fit for calibration of the amperometric
170 signal. After calibration, the K_d of ADP and ATP for Mg^{2+} was determined for each
171 experimental condition by performing multiple titrations with ADP or ATP.

172

173 2.6. *Substrate-uncoupler-inhibitor-titration (SUIT) protocols*

174

175 Coupling control protocols (SUIT-006) assess different coupling control states -
176 LEAK, OXPHOS and ET - at a constant electron-transfer-pathway state (Gnaiger et al
177 2020). The effect of MgG on mitochondrial respiration was evaluated in its absence or
178 presence (1.1 μM), which was added to the experimental chambers prior to sample
179 addition. Since this fluorescent dye is diluted in water, and only a 2 μL volume was added
180 into the 2 mL chamber, no solvent addition was performed in the control group without
181 MgG. After addition of isolated mitochondria into the O2k chambers, residual oxygen
182 consumption Rox was measured in the absence of substrates. Two coupling-control
183 protocols were used to study simultaneously oxygen consumption and ATP production
184 with the following titrations: NADH-pathway with 5 mM pyruvate and 2 mM malate, or
185 Succinate-pathway with 0.5 μM rotenone and 10 mM succinate. First, LEAK respiration
186 was measured in the absence of ADP. Secondly, OXPHOS capacity was measured after
187 addition of 2 mM ADP. Oligomycin (7.5–10.0 nM) or carboxyatractyloside (0.3 – 0.4 mM)
188 were added to induce again a LEAK state. This was followed by stepwise titration of the
189 uncouplers CCCP (0.5 μM steps) or SF 6847 (25–50 nM steps) up to the optimum
190 concentration, when the maximum O_2 flux was achieved as a measure of ET capacity.
191 Finally, residual oxygen consumption was measured after the addition of the CIII inhibitor
192 antimycin A (2.5 μM).

193

194 2.7. *Data analysis*

195

196 The assays were repeated 3 times with independent mitochondrial preparations,
197 with or without MgG, for each condition tested. Data analysis for O_2 consumption,
198 calculations of K_d values and ATP production following Chinopoulos et al 2014, were
199 performed using the templates provided with the software DatLab 7.4.

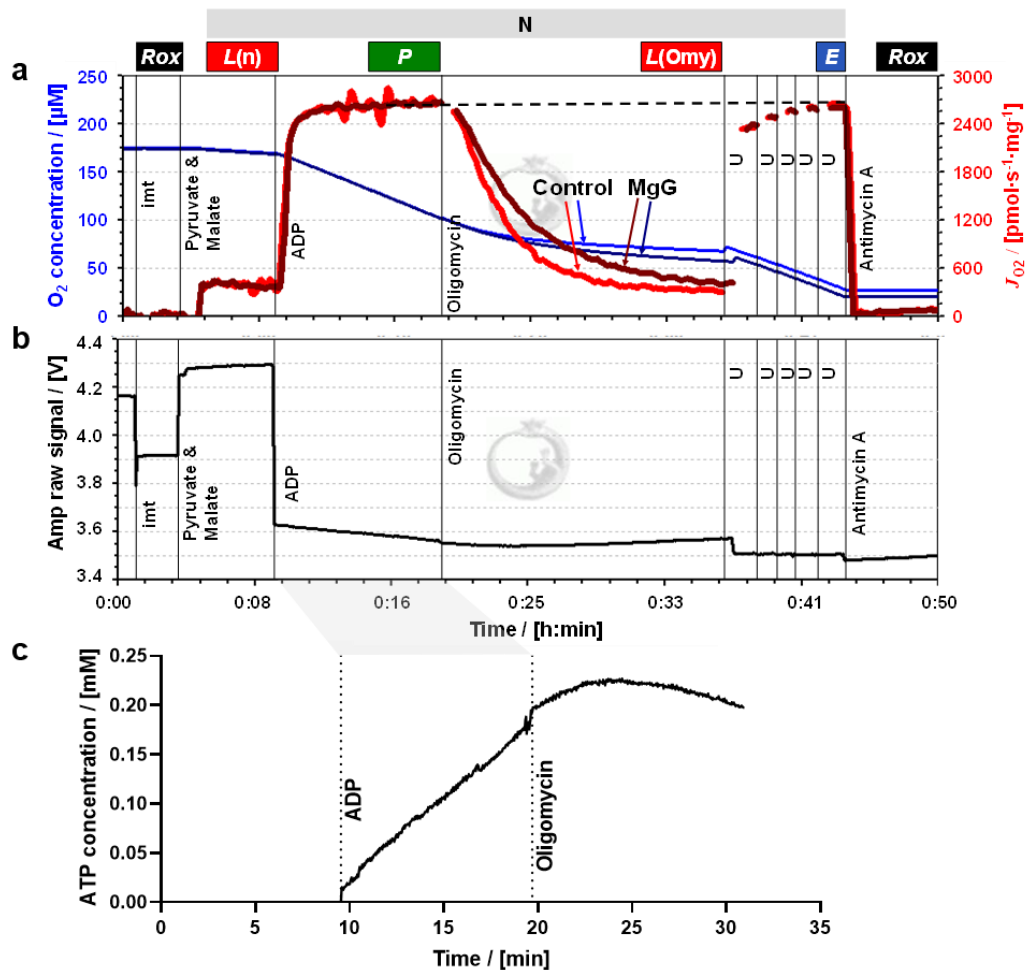
200

201 3. Results and discussion

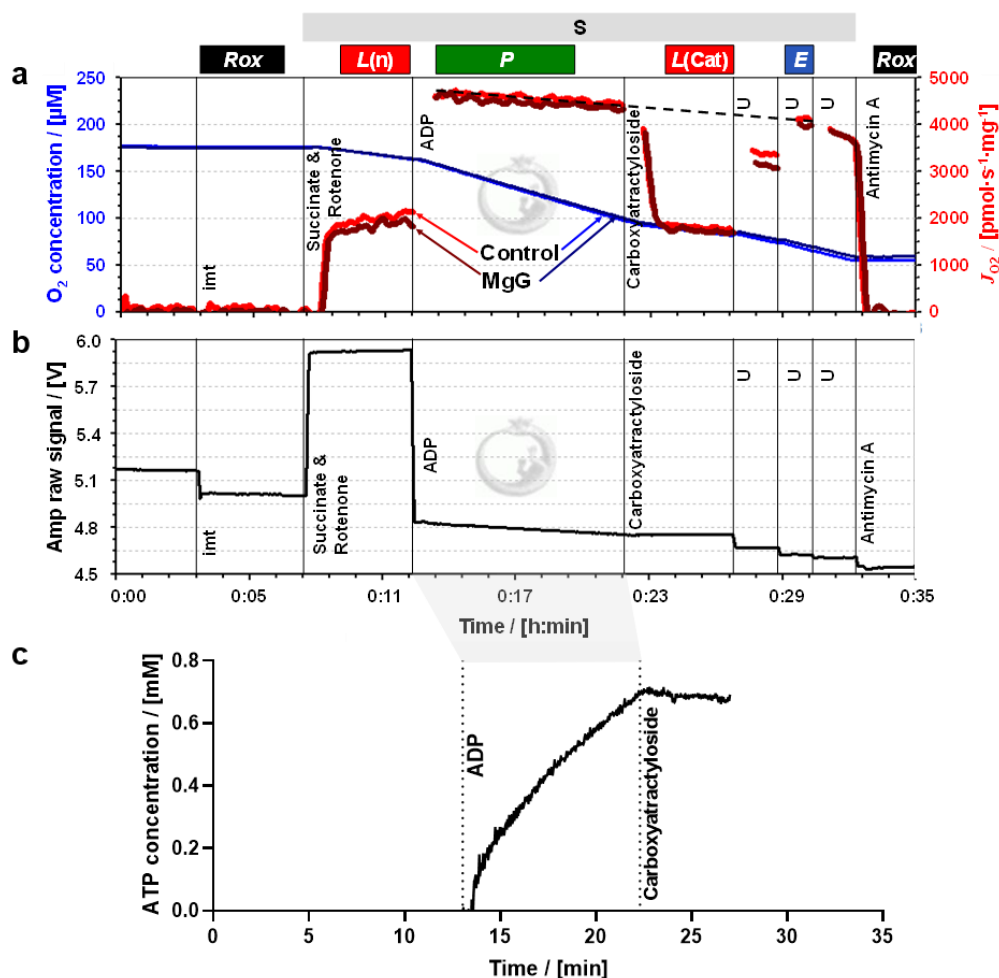
202

203 Figures 2a and 3a show superimposed traces of O_2 concentration and O_2 flux per
204 mass. Coupling control of mitochondrial respiration was measured in two different
205 electron-transfer-pathway control states. In the N-protocol, the NADH-linked pathway
206 through Complex I (CI) was evaluated in the presence of pyruvate and malate which
207 stimulate dehydrogenases of the TCA cycle, leading to reduction of NAD^+ to NADH. NADH
208 is the substrate of CI, with further electron flow into the Q-junction, CIII and CIV (Figure
209 2). In the S-protocol, CI was inhibited by rotenone to prevent reverse electron transfer
210 and accumulation of oxaloacetate, which is an inhibitor of succinate dehydrogenase
211 (Makrecka-Kuka et al 2015; Gnaiger 2020), and respiration was measured supported by
212 succinate as the substrate of CII (Figure 3).

213 In both protocols, LEAK respiration was measured (1) $L(n)$, in the absence of
 214 adenylates and (2) $L(Omy)$ or $L(Cat)$, in the presence of phosphorylation system
 215 inhibitors. Respiration in these two LEAK states was similar, but slightly lower in $L(Omy)$
 216 with the N-protocol (Figure 2a, Table 1). $L(n)$ stabilized quickly, whereas for $L(Omy)$ it
 217 took a long time to fully inhibit respiration by the low concentration of 7.5–10.0 nM
 218 oligomycin. In the S-protocol with sequential addition of rotenone followed by succinate,
 219 $L(n)$ increased for a few minutes until stabilization (Figure 3a). Inhibition by
 220 carboxyatractyloside (0.3–0.4 μM) was immediate, and $L(Cat)$ tended to be slightly lower
 221 than $L(n)$ (Table 1).
 222



223 **Figure 2. Simultaneous measurement of respiration and ATP production by high-**
 224 **resolution Fluorespirometry in mitochondria isolated from mouse heart.**
 225 Representative traces for coupling control protocol SUIT-006 with NADH-linked
 226 substrates (N-protocol), following additions (respiratory states): isolated mitochondria
 227 imt (ROX), pyruvate & malate (LEAK), ADP (OXPHOS), oligomycin (LEAK), uncoupler U
 228 (ET), and antimycin A (ROX). Experiment 2019-02-07 P5 04: **(a)** O_2 concentration (dark
 229 and lighter blue traces) and O_2 flux per mass (dark and lighter red), 1.1 μM MgG versus
 230 control; **(b)** MgG fluorescence signal; **(c)** ATP concentration calculated from MgG signal
 231 calibrated as Mg^{2+} concentration.
 232



233
 234 **Figure 3. Simultaneous measurement of respiration and ATP production by high-**
 235 **resolution Fluorespirometry in mitochondria isolated from mouse heart.**
 236 Representative traces for coupling control protocol SUIT-006 with succinate as substrate
 237 (S-protocol), following additions (respiratory states): isolated mitochondria imt (ROX),
 238 succinate & rotenone (LEAK), ADP (OXPHOS), carboxyatractyloside (LEAK), uncoupler U
 239 (ET), and antimycin A (ROX). Experiment 2019-03-18 P5-03: (a) O_2 concentration (dark
 240 and lighter blue traces) and O_2 flux per mass (dark and lighter red), 1.1 μM MgG versus
 241 control; (b) MgG fluorescence signal; (c) ATP concentration calculated from MgG signal
 242 calibrated as Mg^{2+} concentration.

243
 244 OXPHOS capacity P was measured in the presence of a kinetically saturating
 245 concentration of ADP. The optimum uncoupler concentrations to measure maximum ET
 246 capacity E were 6.0–7.0 μM CCCP in the N-protocol, and 0.150–0.175 μM SF 6847 in the
 247 S-protocol. In the N-protocol, P was stable over time and identical to E . However, in the
 248 S-protocol, P showed a slight decrease over time. Extrapolating this trend of declining O_2
 249 flux to the point where ET capacity was measured explains why E appears to be lower
 250 than P (dashed trendline, Figure 3a). In both protocols, therefore, $E = P$, indicating that
 251 OXPHOS capacity was not limited by the phosphorylation system. This agrees with results

252 for mouse heart mitochondria on coupling control even in the combined NS-pathway
253 (Lemieux et al 2017). Parallel measurements were performed in the presence and
254 absence of 1.1 μM MgG with the N- and S-protocol. This low concentration of MgG used is
255 sufficiently high for calculating ATP production (Figures 2b and c and Figures 3b and c).
256

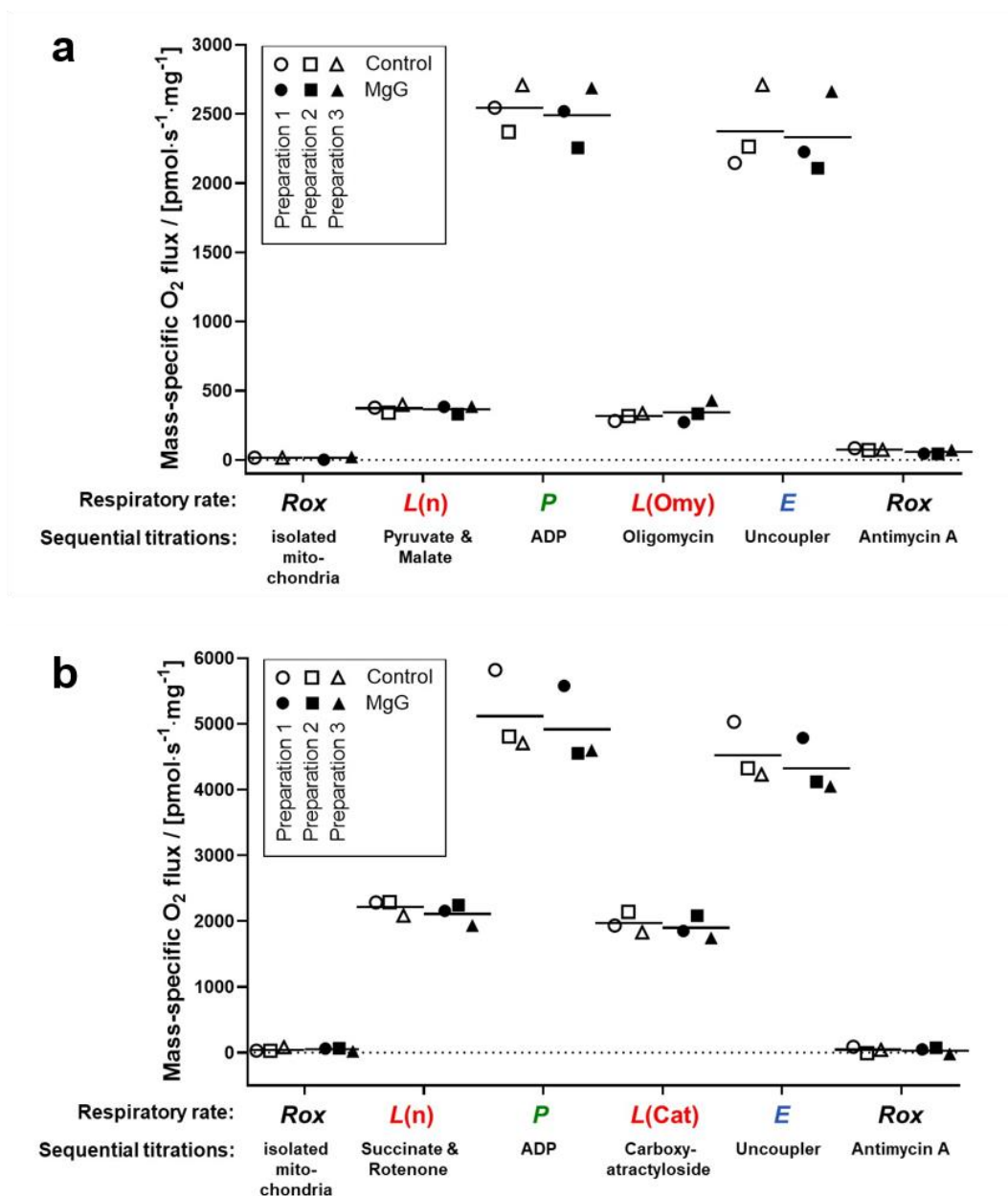
257 The MgG assay to measure ATP production can be used concomitantly with high-
258 resolution respirometry, providing information real-time. Other methods are available to
259 detect ATP production real-time. Spectrophotometric detection of NADPH can be used in
260 conjunction with the coupled enzyme system hexokinase and glucose-6-phosphate
261 dehydrogenase (Horgan, 1978). This assay has been adapted for simultaneous detection
262 of O_2 consumption and NADPH (Lark et al 2016). The luciferin/luciferase assay can be
263 used for continuous measurement of ATP production (Manfredi et al 2002). It is
264 important to note that luciferase consumes O_2 , and instruments typically used for
265 luminometry do not allow monitoring of O_2 concentration in parallel.
266

267 Another method for continuous measurement of the $\text{P}\gg/\text{O}_2$ ratio is the steady-state
268 ADP injection-respirometry (Gnaiger et al 2000b; 2001). The phosphorylation rate is set
269 by continuous injection of ADP as the rate-limiting step while measuring O_2 consumption
270 stimulated to a constant sub-maximal level. Chance and Williams (1955) originally
271 described a polarographic ADP pulse-titration method to determine the $\text{P}\gg/\text{O}_2$ ratio,
272 titrating a known concentration of ADP, which leads to a peak of O_2 consumption
273 stimulated by the complete phosphorylation of ADP to ATP. The ADP pulse-titration
274 method has been extended and critically discussed by Gnaiger (2001).
275

276 End-point assays are available to detect ATP levels, providing discontinuous
277 measurement of ATP production. These include chromatography (high performance
278 liquid chromatography, HPLC; thin layer chromatography, TLC); nuclear magnetic
279 resonance detection of 2-deoxyglucose and its phosphorylated form, and radioactivity
280 measurements using ^{32}P (Menegollo et al 2019; Morciano et al 2017; Fink et al 2017;
281 Sausen et al 2019).
282

283 The fluorometric MgG assay applied simultaneously with O_2 consumption by HRR
284 has been used extensively (Iftikar, Hickey 2013; Goo et al 2013; Chinopoulos et al 2014;
285 Pham et al 2014; Power et al 2014; Salin et al 2016; Napa et al 2017; Masson et al 2017;
286 Salin et al 2018; Devaux et al 2019; Salin et al 2019). Understanding whether MgG may
287 affect respiration is crucial for such studies, particularly for $\text{P}\gg/\text{O}_2$ ratios obtained in
288 different electron-transfer-pathway states.
289

290 It is well established that different dyes commonly applied to measure
291 mitochondrial membrane potential inhibit OXPHOS capacity, *e.g.*, safranin, rhodamine
292 123 and its derivatives TMRM and TMRE (Krumshnabel et al 2014; Scaduto, Grotyohann
293 1999). Surprisingly, Amplex UltraRed used to detect H_2O_2 flux impairs respiration despite
294 not accumulating in the mitochondria (Makrecka-Kuka et al 2015). Therefore, we studied
295 the effect of MgG on respiration. MgG at 1.1 μM did not affect NADH-linked nor succinate-
296 linked respiration in any coupling control state (LEAK, OXPHOS and ET) measured in
297 mitochondria isolated from mouse hearts (Figure 4). In addition, residual oxygen
298 consumption was not affected by MgG.
299



300
 301 **Figure 4. O₂ consumption in the absence and presence of MgG by mitochondria**
 302 **isolated from mouse heart.** The respiratory rates indicated in the abscissa were
 303 measured by HRR with two coupling control protocols SUIT-006, with the following
 304 respiratory states: ROX, LEAK (in the absence of adenylates), OXPHOS, LEAK (in the
 305 presence of inhibitors), ET, and ROX. Sequential titrations are described for **(a)** N-
 306 protocol (experiments 2019-02-05 P3-04, 2019-02-06 P3-03 and 2019-02-07 P5-04) and
 307 **(b)** S-protocol (experiments 2019-03-13 P6-03, 2019-03-14 P3-03 and 2019-03-18 P5-
 308 03). For both graphs the three symbol shapes show independent mitochondrial
 309 preparations, whereas open and closed symbols compare results in controls and in the
 310 presence of MgG from the same preparation; bars represent the average.
 311

312 **Table 1. Coupling control efficiency $(P-L)/P$ and P_{\gg}/O_2 ratio in absence or presence**
 313 **of MgG.** Average \pm SD, $N=3$. OXPHOS capacity P and LEAK respiration L corrected for
 314 residual oxygen consumption Rox . $L(n)/L(inh)$ ratios: L in the absence of adenylates (n)
 315 over L with an inhibitor (inh) of the phosphorylation system, oligomycin Omy or
 316 carboxyatractyloside Cat for the N- or S-pathway, respectively. $L(inh)$ is used in $(P-L)/P$.

Protocol	$(P-L)/P$	$L(n)/L(inh)$	P_{\gg}/O_2	P_{\gg}/O
N-pathway - MgG	0.90 ± 0.01	1.13 ± 0.05	-	-
N-pathway + MgG	0.88 ± 0.02	1.12 ± 0.04	2.33 ± 1.07	1.16 ± 0.53
S-pathway - MgG	0.62 ± 0.05	1.27 ± 0.16	-	-
S-pathway + MgG	0.61 ± 0.05	1.12 ± 0.26	2.78 ± 0.74	1.39 ± 0.37

317
 318 The NADH-pathway has three coupling sites, CI, CIII and CIV, whereas the succinate-
 319 pathway has only the latter two, resulting in a lower P_{\gg}/O_2 ratio. When dividing ATP flux,
 320 calculated from the increase in ATP concentration per time, by the simultaneously
 321 measured O_2 flux, then P_{\gg}/O_2 flux ratios ($J_{P_{\gg}}/J_{O_2}$) are obtained. The P_{\gg}/O_2 is twice the
 322 classical P_{\gg}/O (Table 1). P_{\gg}/O_2 obtained for S-pathway was close to the theoretically
 323 expected value (Gnaiger et al 2020). The result obtained for N-pathway was lower than
 324 expected. A limitation of the present study is the low number of replicates ($N = 3$), with a
 325 high variability of P_{\gg}/O_2 ratios. Further experiments are in preparation.

326
 327 Coupling control efficiencies are closely related to P_{\gg}/O_2 ratios. The coupling
 328 control efficiency is defined as $(E-L)/E$, ranging from 0, at zero coupling, to 1 in a fully
 329 coupled system. In the present case of $P = E$, the coupling control efficiency is expressed
 330 as the $P-L$ control efficiency, $(P-L)/P$ (Gnaiger 2020). As expected, a higher $P-L$ control
 331 efficiency of 0.89 ± 0.02 was found for the N-pathway than 0.62 ± 0.05 for the S-pathway
 332 (pooled data with and without MgG, average \pm standard deviation, $N = 6$; Table 1). These
 333 correspond to a RCR = P/L of 9.6 ± 1.8 for the N-pathway and 2.6 ± 0.3 for the S-pathway.

334
 335 In summary, MgG did not affect respiration in any of the coupling control states.
 336 These results demonstrate that measurement of O_2 consumption is reliable concomitant
 337 with the MgG assay in SUIT protocols with different pathway states and coupling states.
 338

339 Acknowledgements

340 We thank Marco Di Marcello and Manuela Passrigger for expert technical support on media and
 341 chemicals preparation, equipment maintenance and mitochondria isolation. This work was
 342 partially funded by the European Union's Horizon 2020 research and innovation programme
 343 under grant agreement No. 859770, NextGen-O2k project. Contribution to COST Action CA15203
 344 MitoEAGLE.
 345

346 Author contributions

347 LHDC, CD and EG designed the work; LHDC collected and analyzed data and drafted the article;
 348 CD and EG critically revised the article, all authors approved the final version of the manuscript.
 349

350 Conflicts of interest

351 EG is founder and CEO of Oroboros Instruments, Innsbruck, Austria.
 352

353 Data availability

354 Original files are available Open Access at Zenodo repository: [10.5281/zenodo.4032674](https://zenodo.org/record/4032674).

355 Abbreviations

356 Amp amperometric; ANT adenosine nucleotide translocase; BSA bovine serum albumin; CI to CIV
357 Complex I to IV; CCCP carbonyl cyanide m-chlorophenyl hydrazone; $\Delta\Psi_p+$ mt-membrane
358 potential; EGTA ethylene glycol tetraacetic acid; *E* ET capacity; ETS electron transfer system; F_0F_1
359 ATP synthase; Hepes *N*-(2-hydroxyethyl)piperazine-*N'*-(2-ethanesulfonic acid); HRR high-
360 resolution respirometry; imt isolated mitochondria; J_{O_2} O_2 flux; K_d dissociation constant; *L* LEAK
361 respiration; LED light-emitting diode; MES 2-(*N*-morpholino)ethanesulfonic acid hydrate; MgG
362 Magnesium Green; *P* OXPHOS capacity; P_{\gg}/O ADP phosphorylated per atom oxygen consumed;
363 P_{\gg}/O_2 ADP phosphorylated per molecular oxygen consumed; P_i inorganic phosphate; RCR
364 respiratory acceptor control ratio; *Rox* residual oxygen consumption; SUIT substrate-uncoupler -
365 inhibitor-titration; TCA tricarboxylic acid; TMRM tetramethylrhodamine methyl ester; TMRE
366 tetramethylrhodamine ethyl ester; TPP^+ tetraphenylphosphonium; Tris 2-amino-2-
367 (hydroxymethyl)-1,3-propanediol; U uncoupler.
368

369 References

- 370
371 Budinger GRS, Duranteau J, Chandel NS, Schumacker PT (1998) Hibernation during hypoxia in
372 cardiomyocytes. Role of mitochondria as the O_2 sensor. *J Biol Chem* 273:3320-6.
373 Chance B, Williams GR (1955) Respiratory enzymes in oxidative phosphorylation. I. Kinetics of oxygen
374 utilization. *J Biol Chem* 217:383-93.
375 Chinopoulos C, Vajda S, Csanady L, Mandi M, Mathe K, Adam-Vizi V (2009) A Novel Kinetic Assay of
376 Mitochondrial ATP-ADP Exchange Rate Mediated by the ANT. *Biophys J* 96:2490-504.
377 Chinopoulos C, Kiss G, Kawamata H, Starkov AA (2014) Measurement of ADP-ATP exchange in relation to
378 mitochondrial transmembrane potential and oxygen consumption. *Methods Enzymol* 542:333-48.
379 Devaux JBL, Hedges CP, Birch N, Herbert N, Renshaw GMC, Hickey AJR (2019) Acidosis maintains the
380 function of brain mitochondria in hypoxia-tolerant triplefin fish: a strategy to survive acute hypoxic
381 exposure? *Front Physiol* 9:1941.
382 Doerrier C, Garcia-Souza LF, Krumschnabel G, Wohlfarter Y, Mészáros AT, Gnaiger E (2018) High-
383 Resolution FluoRespirometry and OXPHOS protocols for human cells, permeabilized fibers from small
384 biopsies of muscle, and isolated mitochondria. *Methods Mol Biol* 1782:31-70.
385 Fink BD, Bai F, Yu L, Sivitz WI (2017) Regulation of ATP production: dependence on calcium concentration
386 and respiratory state. *Am J Physiol Cell Physiol* 313:C146-53.
387 Fontana M, Krumschnabel G (2015) Isolation of mouse heart mitochondria. *Mitochondr Physiol Network*
388 20.06(01):1-2.
389 Fontana-Ayoub M, Fasching M, Gnaiger E (2016) Selected media and chemicals for respirometry with
390 mitochondrial preparations. *Mitochondr Physiol Network* 03.02(18):1-10.
391 Gnaiger E, Wyss M (1994) Chemical forces in the cell: Calculation for the ATP system. In: *What is Controlling*
392 *Life?* (Gnaiger E, Gellerich FN, Wyss M, eds) *Modern Trends in BioThermoKinetics* 3. Innsbruck Univ
393 Press:207-12.
394 Gnaiger E (2001) Bioenergetics at low oxygen: dependence of respiration and phosphorylation on oxygen
395 and adenosine diphosphate supply. *Respir Physiol* 128:277-97.
396 Gnaiger E (2020) Mitochondrial pathways and respiratory control. An introduction to OXPHOS analysis. 5th
397 ed. *Bioenerg Commun* 2020.2: 112 pp. doi:10.26124/bec:2020-0002.
398 Gnaiger E et al – MitoEAGLE Task Group (2020) Mitochondrial physiology. *Bioenerg Commun* 2020.1.
399 doi:10.26124/bec:2020-0001.v1.
400 Gnaiger E, Kuznetsov AV, Schneeberger S, Seiler R, Brandacher G, Steurer W, Margreiter R (2000a)
401 Mitochondria in the cold. In: *Life in the Cold* (Heldmaier G, Klingenspor M, eds) Springer, Heidelberg,
402 Berlin, New York:431-42.
403 Gnaiger E, Méndez G, Hand SC (2000b) High phosphorylation efficiency and depression of uncoupled
404 respiration in mitochondria under hypoxia. *Proc Natl Acad Sci U S A* 97:11080-5.
405 Goo S, Pham T, Han JC, Nielsen P, Taberner A, Hickey A, Loiselle D (2013) Multiscale measurement of cardiac
406 energetics. *Clin Exp Pharmacol Physiol* 40:671-81.

- 407 Horgan DJ (1978) A spectrophotometric assay of ATP synthesized by sarcoplasmic reticulum. *Aust J Biol Sci*
 408 31:21-4.
- 409 Iftikar FI, Hickey AJ (2013) Do mitochondria limit hot fish hearts? Understanding the role of mitochondrial
 410 function with heat stress in *Notolabrus celidotus*. *PLoS One* 8:e64120.
- 411 Krumschnabel G, Eigentler A, Fasching M, Gnaiger E (2014) Use of safranin for the assessment of
 412 mitochondrial membrane potential by high-resolution respirometry and fluorometry. *Methods Enzymol*
 413 542:163-81.
- 414 Lark DS, Torres MJ, Lin CT, Ryan TE, Anderson EJ, Neuffer PD (2016) Direct real-time quantification of
 415 mitochondrial oxidative phosphorylation efficiency in permeabilized skeletal muscle myofibers. *Am J*
 416 *Physiol Cell Physiol* 311:C239-45.
- 417 Lemieux H, Blier PU, Gnaiger E (2017) Remodeling pathway control of mitochondrial respiratory capacity
 418 by temperature in mouse heart: electron flow through the Q-junction in permeabilized fibers. *Sci Rep*
 419 7:2840, DOI:10.1038/s41598-017-02789-8.
- 420 Leysens A, Nowicky AV, Patterson L, Crompton M, Duchon MR (1996) The relationship between
 421 mitochondrial state, ATP hydrolysis, $[Mg^{2+}]_i$ and $[Ca^{2+}]_i$ studied in isolated rat cardiomyocytes. *J Physiol*
 422 496:111-28.
- 423 Lowry OH, Rosebrough NJ, Farr AL, Randall RJ (1951) Protein measurement with the Folin phenol reagent.
 424 *J Biol Chem* 193:265-275.
- 425 Makrecka-Kuka M, Krumschnabel G, Gnaiger E (2015) High-resolution respirometry for simultaneous
 426 measurement of oxygen and hydrogen peroxide fluxes in permeabilized cells, tissue homogenate and
 427 isolated mitochondria. *Biomolecules* 5:1319-38.
- 428 Manfredi G, Yang L, Gajewski CD, Mattiazzi M (2002) Measurements of ATP in mammalian cells. *Methods*
 429 26:317-26.
- 430 Masson SWC, Hedges CP, Devaux JBL, James CS, Hickey AJR (2017) Mitochondrial glycerol 3-phosphate
 431 facilitates bumblebee pre-flight thermogenesis. *Sci Rep* 7:13107.
- 432 Menegollo M, Tessari I, Bubacco L, Szabadkai G (2019) Determination of ATP, ADP, and AMP Levels by
 433 Reversed-Phase High-Performance Liquid Chromatography in Cultured Cells. *Methods Mol Biol*
 434 1925:223-32.
- 435 Morciano G, Sarti AC, Marchi S, Missiroli S, Falzoni S, Raffaghello L, Pistoia V, Giorgi C, Di Virgilio F, Pinton P
 436 (2017) Use of luciferase probes to measure ATP in living cells and animals. *Nat Protoc* 12:1542-62.
- 437 Napa K, Baeder AC, Witt JE, Rayburn ST, Miller MG, Dallon BW, Gibbs JL, Wilcox SH, Winden DR, Smith JH,
 438 Reynolds PR, Bikman BT (2017) LPS from *P. gingivalis* negatively alters gingival cell mitochondrial
 439 bioenergetics. *Int J Dent* 2017:2697210.
- 440 Pham T, Loisel D, Power A, Hickey AJ (2014) Mitochondrial inefficiencies and anoxic ATP hydrolysis
 441 capacities in diabetic rat heart. *Am J Physiol* 307:C499-507.
- 442 Power A, Pearson N, Pham T, Cheung C, Phillips A, Hickey A (2014) Uncoupling of oxidative phosphorylation
 443 and ATP synthase reversal within the hyperthermic heart. *Physiol Rep* pii:e12138.
- 444 Salin K, Villasevil EM, Auer SK, Anderson GJ, Selman C, Metcalfe NB, Chinopoulos C (2016) Simultaneous
 445 measurement of mitochondrial respiration and ATP production in tissue homogenates and calculation
 446 of effective P/O ratios. *Physiol Rep* 10.14814/phy2.13007.
- 447 Salin K, Villasevil EM, Anderson GJ, Selman C, Chinopoulos C, Metcalfe NB (2018) The RCR and ATP/O
 448 indices can give contradictory messages about mitochondrial efficiency. *Integr Comp Biol* 58:486-94.
- 449 Salin K, Villasevil EM, Anderson GJ, Lamarre SG, Melanson CA, McCarthy I, Selman C, Metcalfe NB (2019)
 450 Differences in mitochondrial efficiency explain individual variation in growth performance. *Proc Biol Sci*
 451 286:20191466.
- 452 Sausen CW, Rogers CM, Bochman ML (2019) Thin-Layer Chromatography and Real-Time Coupled Assays
 453 to Measure ATP Hydrolysis. *Methods Mol Biol* 1999:245-253.
- 454 Scaduto RC Jr, Grotyohann LW (1999) Measurement of mitochondrial membrane potential using
 455 fluorescent rhodamine derivatives. *Biophys J* 76:469-77.

457 **Copyright:** © 2021 The authors. This is an Open Access preprint (not peer-reviewed) distributed
 458 under the terms of the Creative Commons Attribution License, which permits unrestricted use,
 459 distribution, and reproduction in any medium, provided the original authors and source are
 460 credited. © remains with the authors, who have granted MitoFit Preprints an Open Access
 461 publication license in perpetuity.

